SHP-1 phosphatase activity counteracts increased T cell receptor affinity

Michael Hebeisen,[1] Lukas Baitsch,[2] Danilo Presotto,[1] Petra Baumgaertner,[2]
Pedro Romero,[2] Olivier Michielin,[1,2] Daniel E. Speiser,[2] and Nathalie Rufer[1,2]

[1]Department of Oncology, Lausanne University Hospital Center and University of Lausanne, Lausanne, Switzerland.
[2]Ludwig Center for Cancer Research, University of Lausanne, Lausanne, Switzerland.

Anti-self/tumor T cell function can be improved by increasing TCR-peptide MHC (pMHC) affinity within physiological limits, but paradoxically further increases (K_d < 1 μM) lead to drastic functional declines. Using human CD8+ T cells engineered with TCRs of incremental affinity for the tumor antigen HLA-A2/NY-ESO-1, we investigated the molecular mechanisms underlying this high-affinity–associated loss of function. As compared with cells expressing TCR affinities generating optimal function (K_d = 5 to 1 μM), those with supraphysiological affinity (K_d = 1 μM to 15 nM) showed impaired gene expression, signaling, and surface expression of activatory/costimulatory receptors. Preferential expression of the inhibitory receptor programmed cell death-1 (PD-1) was limited to T cells with the highest TCR affinity, correlating with full functional recovery upon PD-1 ligand 1 (PD-L1) blockade. In contrast, upregulation of the Src homology 2 domain-containing phosphatase 1 (SHP-1/PTPN6) was broad, with gradually enhanced expression in CD8+ T cells with increasing TCR affinities. Consequently, pharmacological inhibition of SHP-1 with sodium stibogluconate augmented the function of all engineered T cells, and this correlated with the TCR affinity–dependent levels of SHP-1. These data highlight an unexpected and global role of SHP-1 in regulating CD8+ T cell activation and responsiveness and support the development of therapies inhibiting protein tyrosine phosphatases to enhance T cell–mediated immunity.

Introduction

CD8+ T cell responses rely on the specific recognition by TCRs of small immunogenic peptides presented in the context of MHC class I molecules at the surface of infected or transformed cells. Binding of TCR to peptide-MHC is characterized by relatively low molecular affinity (100 μM to 1 μM) and high specificity and sensitivity, thus enabling T cells to detect rare antigenic epitopes on APCs (1). Due to mechanisms of central and peripheral tolerance, circulating autoreactive T cells recognizing self/tumor-associated antigens typically have TCR–peptide MHC (TCR-pMHC) affinities at the lower end of the physiological range and/or are maintained in unresponsive functional states when compared with pathogen Ag–specific T cells. This might in part explain why tumor-reactive T cell responses detected in cancer patients often fail to control or eliminate advanced disease (2).

Adoptive cell transfer (ACT) of T cells engineered to express TCRs of increased affinity for tumor antigens represents an attractive immunotherapeutic approach to inducing and boosting immune reactivity toward poor immunogenic tumors (3). Numerous studies suggest that enhancing TCR-pMHC interactions (half-life and affinity) would endow T cells with higher functional and protective capacity (4). However, it was also shown that T cells engineered with TCR of very high supraphysiological affinity for pMHC (K_d < 1 nM) lose antigen specificity and become cross-reactive or alloreactive (5–7). As such, TCR optimization through affinity alterations has to include the careful

evaluation of optimal T cell responsiveness to ensure the safety of TCR-engineered T cells in clinical trials (3).
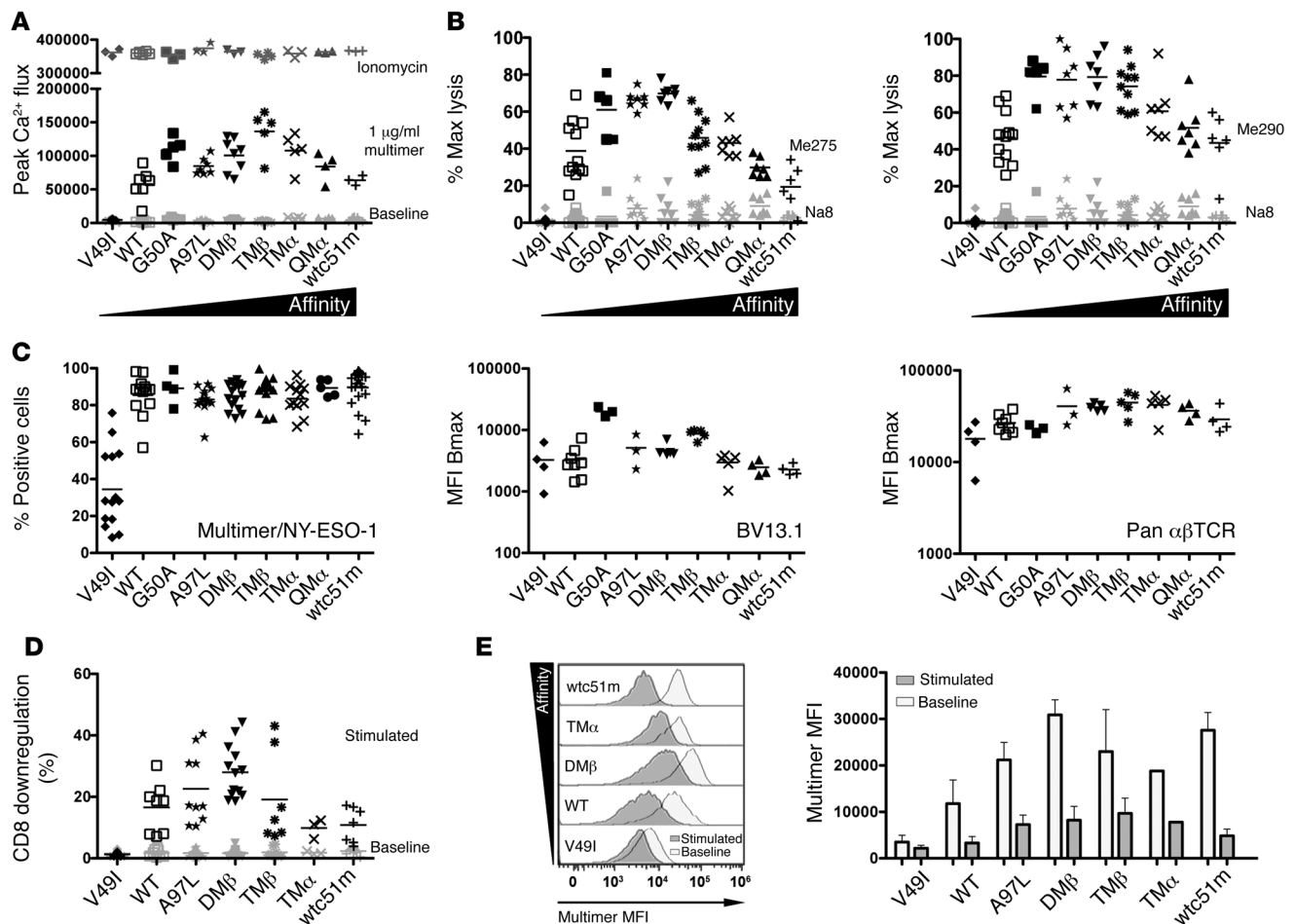
Recently, we characterized the functional impact of TCR-pMHC binding strength by using a panel of human CD8+ T cells engineered through structure-based rationally designed TCRs of incremental affinity for the self/tumor antigen A2/NY-ESO-1$_{157–165}$ (8–11). At low peptide dose stimulation, T cells with TCR affinities ranging in the upper physiological limit (K_d from 5 μM to 1 μM) display higher biological responses, when compared with T cells expressing the WT TCR (K_d at 21.4 μM) (11). Strikingly, tumor-reactive T cells expressing TCRs of supraphysiological affinities (K_d from 1 μM to 15 nM) show drastic functional decline irrespective of CD8 coengagement, which is not associated with loss of antigen specificity (11). Similarly, other studies reported that T cells with TCR-pMHC affinities and/or half-lives extending above the natural range exhibit attenuated T cell activation upon TCR triggering as well as impaired expansion potential and responsiveness (12–16).

To identify the molecular mechanisms underlying these functional defects, we characterized global gene expression, signaling pathways, and activatory/inhibitory membrane receptors on human CD8+ T cells engineered with TCRs of incremental affinity for HLA-A2/NY-ESO-1. We describe how the inhibitory receptor programmed cell death-1 (PD-1) and the Src homology 2 domain–containing phosphatase 1 (SHP-1) are involved in restricting T cell function in TCR-engineered CD8+ T cells. Strikingly, SHP-1 mediated a gradual functional inhibition of CD8+ T cells, along with TCR-binding affinity, independently of PD-1 involvement. Together, these data indicate that, in the context of adoptive cell therapy (ACT), TCR-mediated SHP-1 signaling may counterregulate T cell responses by limiting the potential cytotoxic effect of TCR-optimized CD8+ T cells against self/tumor antigens.

Figure 1
Functionality, TCR-αβ surface expression levels, and TCR/CD8 downregulation in CD8+ T cells engineered with self/tumor-specific TCR of incremental affinities. (**A**) Ca2+ flux of TCR-transduced CD8+ T cells without (baseline) and with 1 μg/ml HLA-A2/NY-ESO–specific multimer stimulation. Maximal Ca2+ flux after ionomycin stimulation indicates equal capacity to mobilize calcium in all T cell variants. Data are expressed as Indo-1 (violet)/Indo-1 (blue) emission ratio. (**B**) Cytotoxic activity (% of maximal killing) against Me 275 and Me 290 (HLA-A2+/NY-ESO-1+) and Na8 (HLA-A2+/NY-ESO-1−) tumor cell lines at an effector target ratio of 10:1. (**C**) Percentage of primary CD8+ T cells expressing the affinity-optimized NY-ESO-1–specific TCRs as detected by A2/NY-ESO-1$_{157–165}$–specific multimer staining (left panel). Cells with greater than 80% multimer labeling were used for further analysis. Surface expression levels (in MFI) of TCR β-chain BV13.1 (middle panel) and total αβTCR (right panel) are shown for all CD8+ transduced T cells. (**D** and **E**) Downregulation of CD8 coreceptor (**D**; in %) and TCR (**E**; in MFI) in engineered CD8+ T cells in the absence (baseline) or presence of 0.1 μg/ml unlabeled A2/NY-ESO-1–specific multimer. Data from T cells with reduced CD8 expression (**D**; CD8 low) are shown as percentage of total T cells (CD8 high and low). TCR downregulation following stimulation (**E**) is depicted as dark gray histograms or columns. Error bars represent mean ± SD.

Results

Impaired function of human primary CD8+ T cells expressing self/tumor-specific TCRs of supraphysiological affinity. Using a panel of affinity-optimized HLA-A*0201-restricted NY-ESO-1$_{157–165}$-specific TCR (BC1) variants with gradually increased affinity of up to 1400-fold from the native TCR (refs. 8, 9, and Supplemental Table 1; supplemental material available online with this article; doi:10.1172/JCI65325DS1), we previously found that maximal biological activity occurred within a well-defined affinity window with K_d ranging from 5 to 1 μM (10, 11). Importantly, under low-peptide stimulation conditions, cellular activity, including Ca2+ mobilization capacity (Figure 1A) and tumor cell killing (Figure 1B), was globally attenuated for T cells expressing either TCRs of very low (K_d >100 μM; V49I) or of supraphysiological (K_d < 1 μM; TMα,

QMα, and wtc51m) affinities. Conversely, high concentrations of NY-ESO-1$_{157–165}$ peptide loaded on APCs restored the Ca2+ mobilization capacity of CD8 T cells with supraphysiological TCRs (Supplemental Figure 1), consistent with our recent report (11). Similar data were obtained independently of stimulation with peptide-pulsed APCs or A2/peptide multimers. This functional decline was not caused by lower TCR expression, as engineered CD8+ T cells and α-TCR knockout SUP-T1 cells expressed comparable surface levels of TCR-β chain (BV13.1) and of overall TCR-αβ chains (Figure 1C and Supplemental Figure 2A).

Upon short-term peptide stimulation, we observed substantial TCR downregulation (reduced multimer fluorescence; Figure 1E) in all engineered CD8+ T cells independently of their TCR affinities (e.g., optimal versus supraphysiological). TCR downmodula-
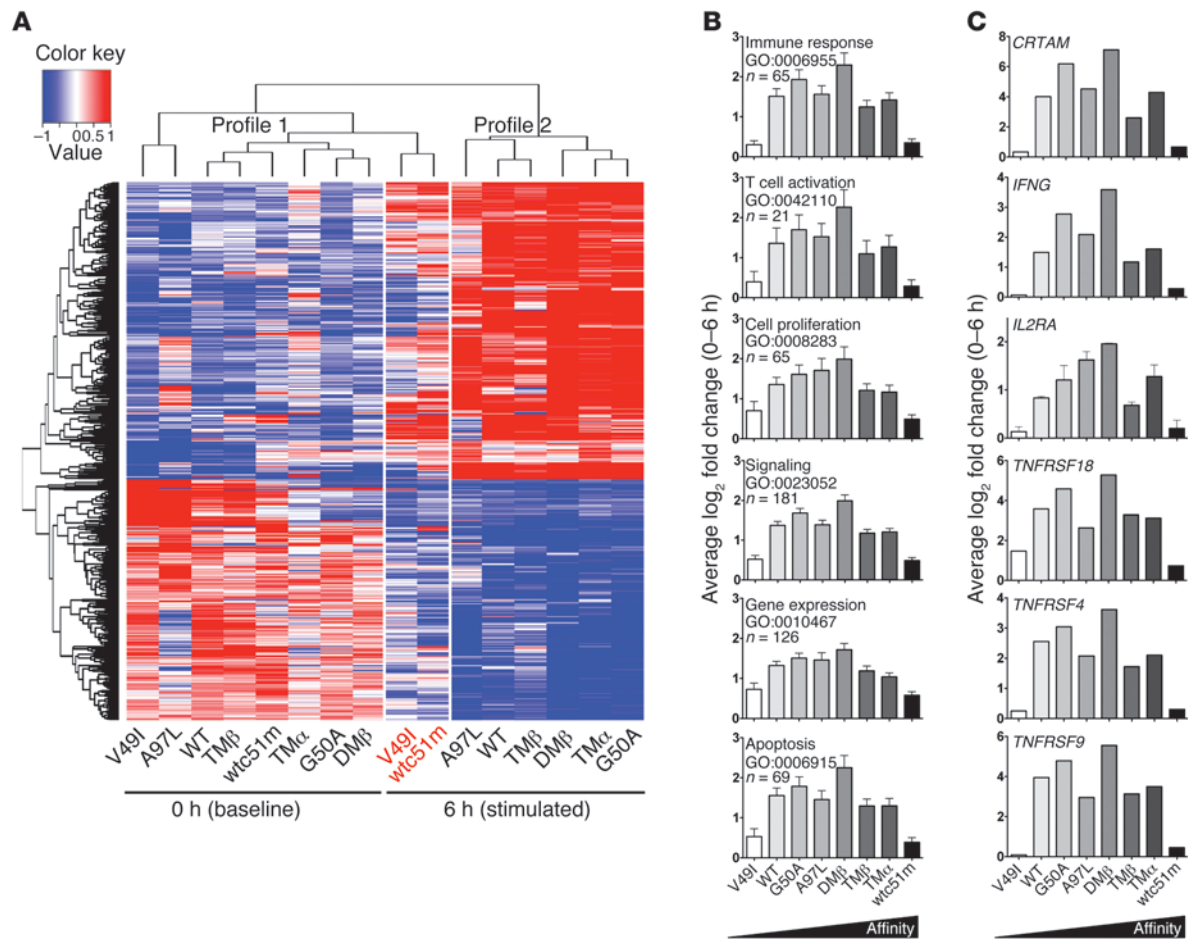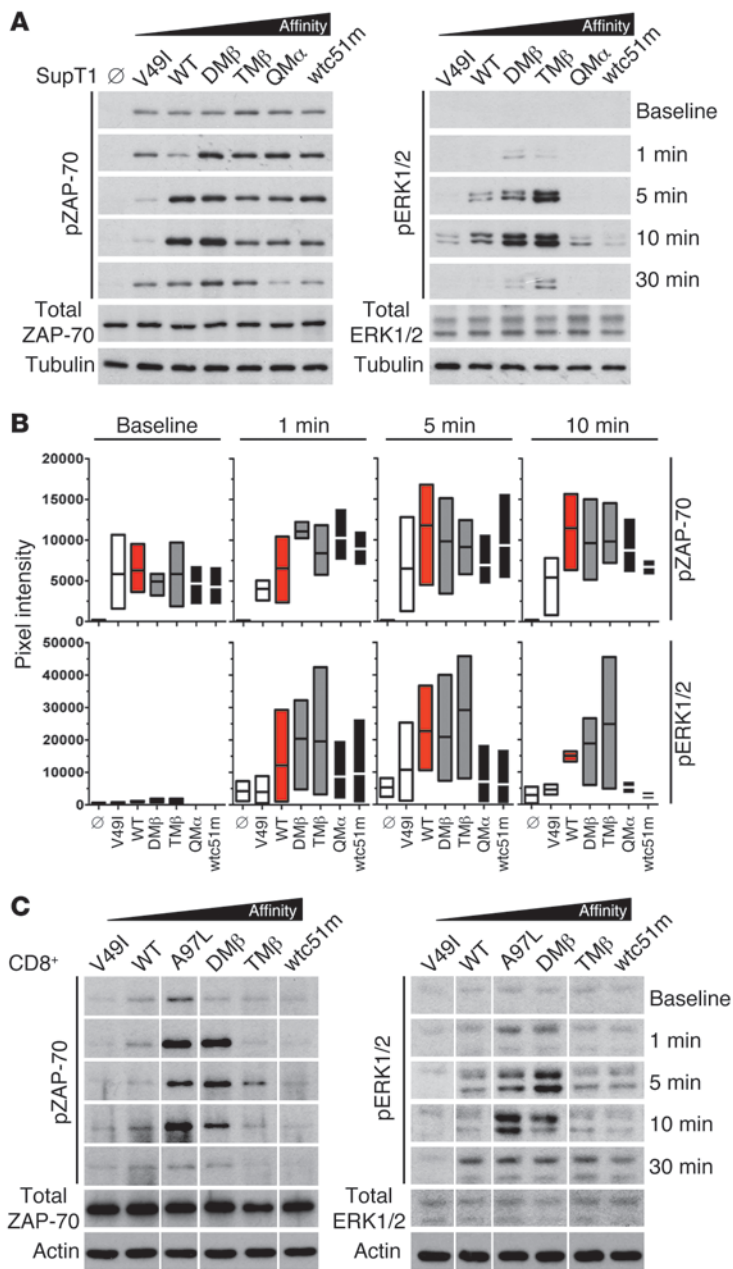
Figure 2

Gene expression of CD8^{+} T cells engineered with TCR of incremental affinities. (**A**) Microarray hierarchical clustering of gene expression intensities from the 538 gene probes with statistically significant changes in expression values (> 2-fold and adjusted *P* < 0.05) after 6-hour stimulation with unlabeled A2/NY-ESO-1–specific multimer (0.002 μg/ml) separated the samples in 2 profiles shown above the heat map. Upregulated probes are shown in red, downregulated in blue. Expression profiles of genes from CD8^{+} T cells transduced with either very low (V49I) or very high (wtc51m) affinity TCRs, after 6-hour stimulation (names depicted in red) cluster together within the unstimulated (0 hour) profile 1 group. (**B**) 524 genes enriched between 0 and 6 hours in T cells transduced with TCRs giving maximal function (G50A, A97L, DMβ, TMβ) could be classified using GOTermFinder. (**C**) Log2-fold changes in the expression levels of representative TCR response genes (*CRTAM*, *IL2RA*), T cell effector cytokine (*IFNG*), and costimulatory molecules (*TNFRSF18* [GITR], *TNFRSF4* [OX40], *TNFRSF9* [4-1BB]).

tion was assessed either by multimer fluorescence (Figure 1E) or by staining with anti-BV13 mAbs (Supplemental Figure 2). In contrast, reduced CD8 coreceptor expression (Figure 1D and Supplemental Figure 2) was primarily found in T cells expressing TCRs mediating maximal/optimal function (A97L, DMβ, TMβ) rather than in T cells of supraphysiological TCR affinity (TMα, wtc51m). Altogether, our data further emphasize the paradoxical status of these NY-ESO-1–specific T cells expressing very high TCR affinities with impaired functionality despite retaining robust surface-binding TCR avidity and TCR downregulation capacity upon stimulation (Figure 1 and refs. 10, 11). These findings suggest the presence of potential mechanisms controlling T cell activation, signaling, and subsequent functionality.

Altered gene expression profiles in CD8^{+} T cells with TCRs of supraphysiological affinity following antigen-specific stimulation. In order to uncover the molecular mechanisms involved in the impaired functional responsiveness of cells bearing supraphysiological TCRs, we

performed a genome-wide microarray analysis on primary CD8^{+} T cells expressing the panel of TCR variants following low-dose A2/NY-ESO-1–specific multimer stimulation (Figure 2A). We compared the global gene expression levels of all samples before and after 6 hours of stimulation, and found 538 gene probes showing at least a 2-fold differential expression (data not shown). Similar gene expression patterns were observed between engineered T cells belonging to the same culture conditions (unstimulated versus 6-hour stimulated) and could accordingly be defined within 2 distinct clusters or profiles. However, unsupervised hierarchical clustering revealed that the 6-hour–stimulated T cells expressing infra- (V49I) and supraphysiological (wtc51m) affinity TCRs both clustered with the unstimulated T cells (Figure 2A).

To obtain a gene signature of optimal T cell activation, we compared the gene expression profiles of the 4 TCR-transduced CD8^{+} T cells known to produce maximal function (G50A, A97L, DMβ, TMβ) before and after 6-hour activation. With this strategy, we
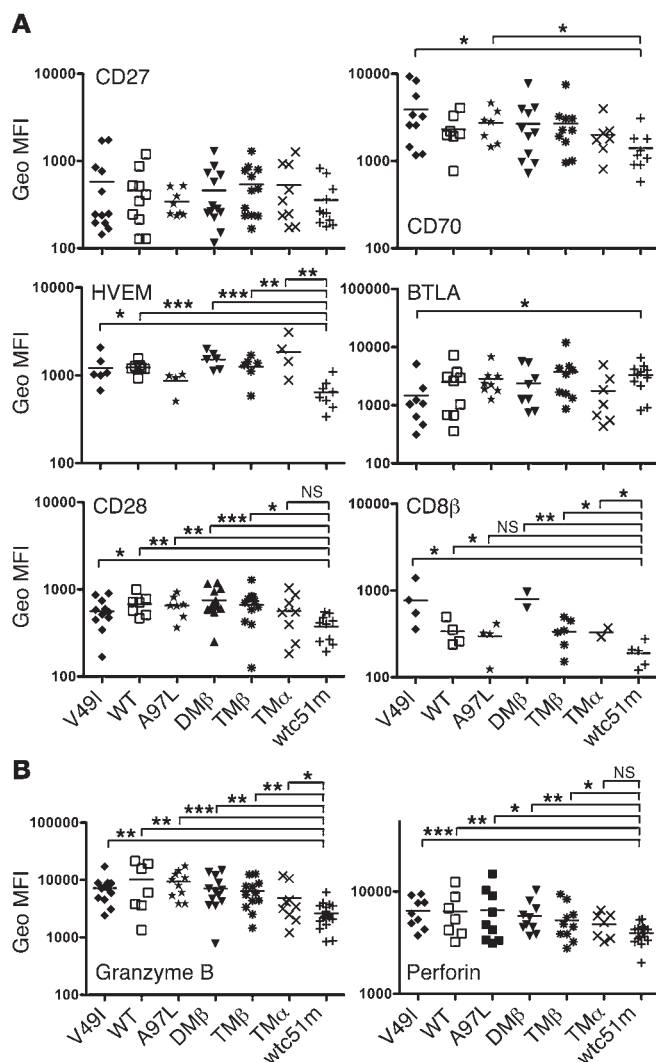
Figure 3
Levels of ZAP-70 and ERK 1/2 phosphorylation in SUP-T1 and CD8+ T cells engineered with TCRs of incremental affinities. (**A** and **C**) TCR-transduced SUP-T1 T cells (**A**) and CD8+ T cells (**C**) were stimulated with 10 µg/ml A2/NY-ESO-1$_{157–165}$ multimers at 37°C for the indicated time points. Total ZAP-70 and ERK 1/2 are shown as internal controls, while α-tubulin (**A**) or actin (**C**) expression levels were used as loading controls between samples. Data are each representative of 3 independent experiments. TCR-untransduced SUP-T1 cells are shown as empty controls (Ø). For CD8+ T cells, all lines were run on the same gel but were noncontiguous. (**B**) To allow direct comparison between the different SUP-T1–transduced TCR variants, intensity of ZAP-70 and ERK1/2 phosphorylation levels were quantified and normalized to α-tubulin. Data from 3 independent experiments are presented as min-to-max bar graphs with average mean lines.

identified 524 differentially expressed genes and classified them according to 6 general Gene Ontology (GO) terms. The average absolute log$_2$ fold change (0 to 6 hours) of the genes within each GO term is represented in Figure 2B. Remarkably, all GO terms (immune response, T cell activation, cell proliferation, signaling, gene expression, and apoptosis) had the same overall outline demonstrating a drastic underrepresentation of the gene expression within V49I and wtc51m TCR variants. The average absolute fold change was progressively increased from low to optimal TCR affinity before declining in T cells with supraphysiological TCR variants (TMα and wtc51m). Interestingly, the pattern of gene expression profile related to apoptosis strongly correlated to the one observed following A2/peptide multimer stimulation and staining with Annexin V (11), with highest levels of apoptosis for CD8+ T cells expressing optimal TCRs. In addition, several key genes involved in T cell activation (e.g., *CRTAM*, *IFNG*, and *IL2RA*) as well as costimulatory molecules (e.g., *TNFRSF18*, *TNFRSF4*, *TNFRSF9*) showed a 2-fold or greater change and displayed the same overall bell-shape profile following 6-hour stimulation (Figure 2C). No major changes in genes classified to the GO terms were observed at baseline in unstimulated CD8+ T cells (Supplemental Figure 3).

Similar to the functional data (Figure 1), gene expression analyses revealed that T cells engineered with TCR of infra- or supraphysiological affinity clustered together and failed to properly modulate their transcriptome upon specific TCR triggering. Conversely, the transcriptional gene signatures of CD8+ T cells expressing optimal TCR variants (G50A, A97L, DMβ, and TMβ) revealed drastic global changes (up- or downregulation) in gene expression levels following short-term antigen-specific stimulation, supporting enhanced T cell responsiveness.

Affinity of TCR-pMHC interaction affects the intensity and duration of TCR-mediated intracellular signaling. To gain functional insights into the molecular mechanisms underlying altered gene expression profiling associated with very low or very high TCR affinities (Figure 2), we explored the impact of TCR affinity on cell signaling. We assessed the activation levels of ZAP-70, a proximal activatory molecule of TCR signaling and of the distal MAPK family members ERK1/2 (p38). SUP-T1 and CD8+ T cells expressing TCR variants were stimulated with A2/NY-ESO-1–specific multimers and levels of phosphorylated ZAP-70 (pY319) and ERK1/2 (pT202/pY204 ERK1; pT185/pY187 ERK2) were quantified in kinetic analyses. Upon specific stimulation, we found differential levels of ZAP-70 phosphorylation intensity and duration correlating with TCR affinity variants (Figure 3 and Supplemental Figure 4). V49I-transduced T cells showed only transient and low levels of ZAP-70 phosphorylation, whereas cells expressing TCR variants mediating optimal functions (e.g., A97L, DMβ) generated fast and sustained ZAP-70 phosphorylation. Importantly, in CD8+ (Figure 3C and Supplemental Figure 4) and SUP-T1 (Figure 3, A and B) cells expressing supraphysiological TCR affinities (e.g., QMα and wtc51m), ZAP-70 phosphorylation declined rapidly and substantially following specific stimulation.

Figure 4
Surface expression of costimulatory molecules and coactivatory/inhibitory receptors in CD8+ T cells engineered with TCR of incremental affinities. (**A**) Surface expression levels of the TNFR-TNFR ligand pairs (i) CD27-CD70 and (ii) HVEM-BTLA as well as of CD28 and CD8β are shown in steady-state conditions (unstimulated cells). TCR variants are presented in order of increased affinity. Data were obtained from 10 independent experiments. (**B**) Baseline expression levels of Granzyme B and Perforin in CD8+ T cells transduced with TCR variants. Data were obtained from 7 independent experiments. (**A** and **B**) Unpaired 2-tailed t test; ***$P < 0.001$; **$P < 0.01$; *$P < 0.05$.

ERK1/2 phosphorylation profiles corresponded with those observed for ZAP-70 phosphorylation, with an overall increase in the signaling intensities depending as well on the TCR affinity variants. Maximal phosphorylation was found for TCR variants of optimal function, while T cells with supraphysiological TCRs showed mostly a transient and rapid loss of ERK1/2 phosphorylation following TCR stimulation (Figure 3 and Supplemental Figure 4). Together, the transgenic TCR affinity strongly affected both the intensity and the duration of ZAP-70 and ERK1/2 phosphorylation. Importantly, CD8+ T cells expressing supraphysiological TCR affinity presented a drastically reduced activation of

key TCR downstream signaling pathways (Ca^{2+} and MAPK), and this occurred at a very proximal step in the TCR-signaling cascade (ZAP-70). Conversely, the low cell signaling observed in V49I-expressing T cells nicely correlated with the poor intrinsic binding avidity of this particular TCR (10, 11).

Impact of TCR-pMHC affinity on the expression of coactivatory/inhibitory receptors. Since global genome profiling revealed reduced expression of genes involved in costimulatory/activatory molecules in supraphysiological T cells (Figure 2), we next focused on measuring the surface expression levels of CD28 as well as CD27 and HVEM and their respective ligands (CD70 and BTLA) (Figure 4A). Under steady-state conditions, most of the TCR-transduced CD8+ T cells, including cells with the lowest TCR affinity variant (V49I), expressed similar levels of CD28 as well as of CD27 and HVEM with their respective ligands. Strikingly, T cells bearing supraphysiological TCR affinity (wtc51m) had substantially lower expression of CD28, HVEM, CD70, all 3 involved in T cell activation signaling. In contrast, BTLA, known to inhibit T cell function (17), was expressed at the highest levels in wtc51m-expressing T cells (Figure 4A). No significant differences in CD8α expression were found (data not shown), yet there was a trend of lower expression of CD8β in T cells with supraphysiological TCRs (Figure 4A). Significantly reduced expression of Granzyme B and Perforin (Figure 4B) was also found in the latter T cells (wtc51m), consistent with their attenuated killing capacities (Figure 1B). Importantly, similar data were obtained when CD8+ T cells were stimulated with A2/NY-ESO-1–specific multimers over a 24-hour and 48-hour period of time (data not shown). Overall, these data further support the notion that CD8+ T cells expressing supraphysiological TCR affinities likely exhibit molecular mechanisms that actively downregulate surface coactivatory molecules/receptors. This was readily observed under steady-state conditions.

Engineered T cells of supraphysiological TCR affinity show enhanced expression of PD-1 correlating with full functional recovery upon PD-L1 blockade. CD8+ T cells express multiple negative regulators, such as BTLA, PD-1, and CTLA-4, which have been proposed to play central roles in preventing uncontrolled T cell activation and autoimmunity during inflammatory responses (18). Therefore, we sought to determine whether PD-1 could functionally regulate CD8+ T cells expressing TCRs of increased affinities. We assessed PD-1 expression in unstimulated TCR-engineered T cells (Figure 5, B and C). Comparable with mRNA data (Figure 5A), elevated PD-1 levels were exclusively found in CD8+ T cells of highest supraphysiological affinity (wtc51m). Of note, *PD1* mRNA fold-change at 6-hour stimulation showed the same overall bell-shape profile with maximal expression in T cells mediating optimal function (A97L, DMβ, and TMβ), thereby indicating that PD-1 expression can also be induced shortly after antigen-specific TCR stimulation (Figure 5A). No significant differences were found in expression levels of PD-1 ligand 1 (PD-L1) (Figure 5B) and CTLA-4 (data not shown).

Since PD-L1 surface expression was highly comparable across the TCR affinity panel, we next evaluated the biological significance of PD-1 expression on T cell responsiveness by blocking PD-1/PD-L1 interaction. All transduced CD8+ T cells were incubated with PD-L1 neutralizing antibody prior to LAMP1/CD107a degranulation assays (Figure 5, D and E). After 4-hour triggering with the NY-ESO-1 peptide, PD-L1 blockade had no effect on CD107a degranulation in most of CD8+ T cells, with the exception of the supraphysiological TCR variant (wtc51m), which exhibited an increased proportion of degranulating cells, even reaching lev-
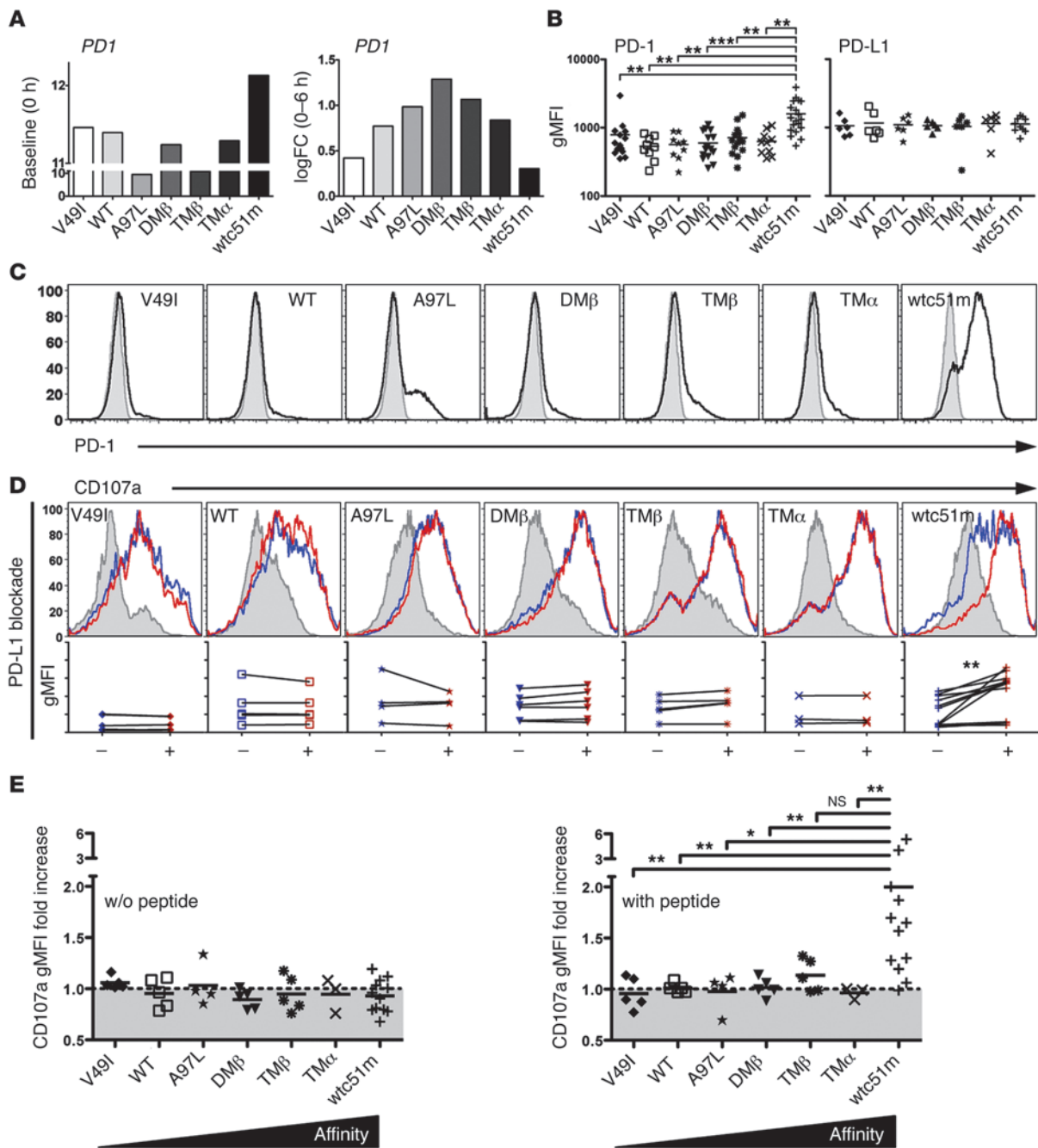
Figure 5

PD-1 expression in TCR-engineered CD8+ T cells and functional impact of PD-L1 blockade. (**A**) Unstimulated at baseline (0 hour) and $\log_2$ fold change (0–6 hours) expression levels of *PD1* transcripts as detected in microarray analysis. (**B**) Average surface expression of PD-1 ($n > 9$ independent experiments) and its ligand PD-L1 ($n > 6$ independent experiments) of TCR-engineered CD8+ T cells. Unpaired 2-tailed t test; ***$P < 0.001$; **$P < 0.01$. (**C**) Representative histograms of PD-1 surface expression (in MFI) in TCR-engineered CD8+ T cells under steady-state conditions. (**D**) Representative histograms of levels (in MFI) of the degranulation marker LAMP-1/CD107a in TCR-transduced CD8+ T cells without (control, blue histograms) or with PD-L1 blocking antibody (red histograms) prior to 4-hour stimulation with 10 μM NY-ESO-1$_{157-165}$–loaded T2 cells. CD107a degranulation following stimulation with unloaded T2 cells is depicted as gray histograms. Graphs below each respective histogram represent the direct comparison of TCR stimulation–associated CD107a levels without (–) or with PD-L1 blockade (+). Data were obtained from more than 4 independent experiments. Paired 2-tailed t test, **$P < 0.01$. (**E**) Relative CD107a degranulation ratio (in gMFI) obtained in the presence versus the absence of PD-L1 blocking antibody. Graphs are depicted as relative CD107 fold increase following stimulation with unloaded (left panel) or NY-ESO-1–pulsed (right panel) T2 cells. Unpaired 2-tailed t test; **$P < 0.01$; *$P < 0.05$.

A SHP1

B CD8+ / pSHP-1 / Actin — Total SHP-1 / Actin
Baseline, 1 min, 5 min, 10 min, 30 min

C SupT1 / pSHP-1 / Tubulin — Total SHP-1 / Tubulin
Baseline, 1 min, 5 min, 10 min, 30 min
Affinity

D Baseline / 5 min / 10 min / 30 min — pSHP-1 / Total SHP-1 — Pixel intensity

E miR-181a / miR-155 / BIC — Relative miR expression / Signal intensity

Figure 6

Levels of SHP-1 protein and of miR-155 and miR-181a expression in CD8+ T cells engineered with TCRs of incremental affinities. (**A**) Unstimulated at baseline (0 hours) and $\log_2$ fold change (0–6 hour difference) expression levels of *SHP1* transcripts as detected in microarray analysis. (**B** and **C**) TCR-transduced CD8+ T cells (**B**) and SUP-T1 cells (**C**) were stimulated with 10 μg/ml A2/NY-ESO-1$_{157-165}$ multimers for the indicated time points and assessed for SHP-1 phosphorylation and total SHP-1 levels by Western blotting. Actin (**B**) or α-tubulin (**C**) expression levels were used as loading controls between samples. Data are each representative of 3 independent experiments. For CD8+ transduced T cell samples, all lines were run on the same gel, but were noncontiguous. TCR-untransduced SUP-T1 cells are shown as empty controls (Ø). (**D**) To allow direct comparison between the engineered SUP-T1 cells, intensity of SHP-1 phosphorylation and of total SHP-1 levels was quantified and normalized to α-tubulin (*n* = 3 independent experiments). (**E**) Expression levels of miR-181a and miR-155 were determined by qRT-PCR in TCR-transduced CD8+ T cells following stimulation with 0.1 μg/ml A2/NY-ESO-1$_{157-165}$ multimers at the indicated time points. Data represent relative expression compared with RNU48 control and are representative of 3 independent experiments. Pri-miR-155 (BIC) mRNA expression values (inset) were retrieved from the microarray analysis.

els similar to those of the other TCR variants (Figure 5D). Relative CD107a degranulation activity further confirmed that blocking the PD-1/PD-L1 pathway led to full functional recovery in the supraphysiological T cells (Figure 5E). Collectively, our data revealed preferential expression of PD-1 in supraphysiological CD8+ T cells, i.e., those with TCRs in the nanomolar range (wtc51m). Furthermore, PD-L1 blockade restored CD107a degranulation in PD-1^{hi-} expressing cells, demonstrating its key implication in the functional regulation of those T cells.

Enhanced expression of SHP-1 phosphatase in a TCR affinity–dependent manner. SHP-1 and SHP-2 phosphatases can be recruited by multiple inhibitory surface receptors in T cells and may inhibit TCR signaling (19) through dephosphorylation of proximal signaling targets (e.g., LCK, ZAP-70, CD3ζ). Under unstimulated conditions, *SHP1* gene expression was progressively increased from low to high TCR affinity (Figure 6A; baseline). We characterized the expression levels of total SHP-1 protein and its phosphorylated activatory form Y536 (20) as well as those of total SHP-2 protein (Figure 6 and Supplemental Figure 5). Maximum levels of SHP-1 phosphorylation were detected in both CD8+ and SUP-T1 T cells transduced with supraphysiological TCR variants (e.g., QMα and wtc51m) after antigenspecific stimulation and already under steady-state conditions. Importantly, transient levels of phosphorylated SHP-1 were also enhanced in the other TCR variants upon stimulation, yet never reached those observed in QMα- and wtc51m-transduced T cells. Total SHP-1 protein revealed expression patterns that followed the same TCR binding hierarchy, with intermediate and highest levels found for optimal and supraphysiological TCR affinities, respectively (Figure 6). In CD8+ T cells, the weak binding TCR ligand V49I was also able to trigger SHP-1 protein expression and phosphorylation, consistent with a previous report (21) showing that SHP-1 is involved in antagonist-mediated inhibition. Thus, differing from PD-1 expression, SHP-1 phosphatase was found upregulated in a TCR affinity–dependent manner with substantial expression levels readily found in T cells of optimal TCR affinities. A comparable trend was observed for total SHP-2 expression (Supplemental Figure 5).

Finally, we assessed the expression levels of miR-181a and miR-155 (Figure 6E), 2 microRNAs, mostly known to affect, respectively, lymphocyte development and function (22, 23). Following specific TCR stimulation, only minor changes in miR-181a expression were found within the engineered panels of CD8+ T cells. This highly contrasted with the strong induction in pri-miR-155 (BIC transcript) and miR-155 expression observed within T cells expressing WT and optimal TCR affinities (e.g., A97L, DMβ).

Impact of pharmacological SHP-1 phosphatase inhibition on degranulation and cytotoxicity of TCR engineered CD8+ T cells. Sodium stibogluconate (SSG) is widely used to treat visceral leishmaniasis and was recently identified as an important clinically suitable protein tyrosine phosphatase inhibitor in cancer patients (24, 25). Notably, SSG has been shown to selectively inhibit protein tyrosine phosphatases, among which SHP-1 was the most sensitive (26). Given the elevated levels of SHP-1 and SHP-2 protein expression within engineered CD8+ T cells, we next determined whether SSG treatment might improve their function, irrespectively of PD-1 expression (Figure 7). We incubated the CD8+ T cells in the presence or absence of SSG for 3 days at a concentration (50 μg/ml) shown to partially inhibit SHP-2 activity as well (26). Following pharmacological inhibition of SHP-1/SHP-2, increased degranulation potential (Figure 7, A and B) was found within the whole T cell panel, except for cells expressing the infraphysiological TCR affinity V49I. Importantly, functional recovery was further validated in target cell killing experiments (Figure 7, C and D) and correlated well with the affinity-dependent levels of SHP-1 phosphatase found in T cells. Indeed, and in agreement with their stronger phosphorylation levels, supraphysiological T cells showed better killing recovery capacity when compared with WT and optimal T cells. Although we cannot formally exclude offtarget effects of SSG treatment, these results support the notion that SHP-1 phosphatase (and eventually SHP-2) may mediate a gradual functional inhibition in TCR-engineered CD8+ T cells depending on TCR affinity, but not necessarily on the degree of PD-1 involvement.

Discussion

The panel of rationally designed NY-ESO-1$_{157-165}$–specific TCRs with incremental affinity (8, 9) provides a unique model for investigating the relationship between TCR affinity and T cell function as well as its modulation by activatory/inhibitory coreceptors and their signaling pathways. Here, we show that the impaired functionality recently observed in CD8+ T cells engineered with supraphysiological TCR affinities ($K_d < 1$ μM) (11) was associated with a strong decrease in overall gene expression profile, intracellular signaling, and surface expression of activatory TNFR superfamily members (Figures 2, 3, and 4). Our major findings revealed that the T cell effectiveness of engineered CD8+ T cells was limited by at least 2 mechanisms. The first one was characterized by the preferential expression of PD-1 inhibitory receptor within T cells of highest supraphysiological TCR affinity (wtc51m variant), and this correlated in those cells with restored cell responsiveness upon PD-1/PD-L1 blockade (Figure 5). The second one was associated with the gradual increased expression of SHP-1 phosphatase in a TCR affinity–dependent manner, from WT to very high TCR affinities (Figure 6). In contrast to PD-1/PD-L1 blockade experiments, pharmacological inhibition using SSG known to inhibit SHP-1 (and partially SHP-2) allowed further incremental gaining of cell function in engineered CD8+ T cells according to their TCR-binding affinity (Figure 7).
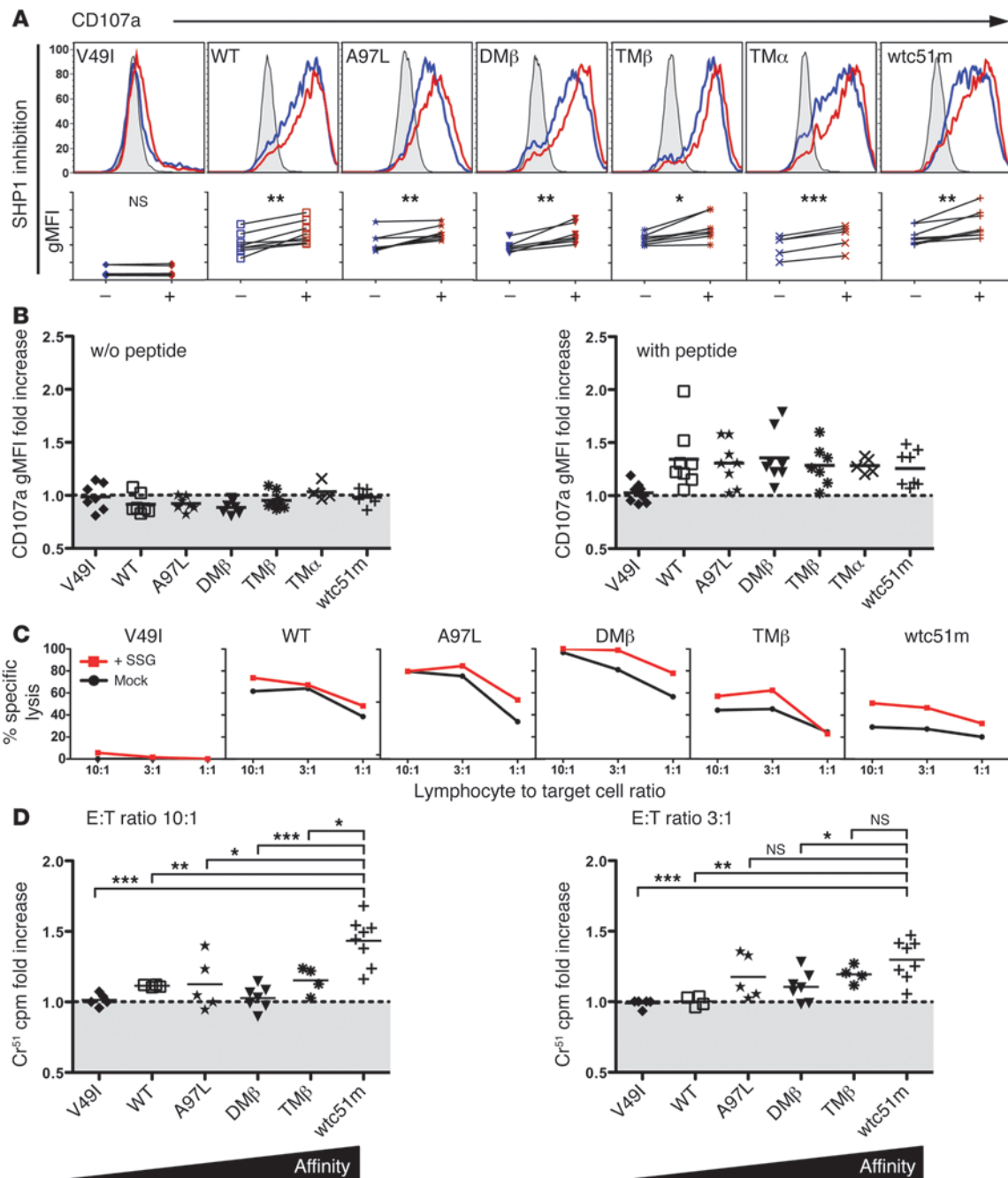
Figure 7

Pharmacological inhibition of SHP-1 phosphatase in TCR engineered CD8+ T cells. (**A**) Representative histograms of the levels (in MFI) of LAMP-1/CD107a expression in TCR-transduced CD8+ T cells without (control, blue histograms) or with SHP-1 inhibition by SSG (red histograms) prior to 4 hour stimulation with 10 μM NY-ESO-1$_{157-165}$–loaded T2 cells. CD107a degranulation following stimulation with unloaded T2 cells is depicted as gray histograms. Graphs below each respective histogram represent the direct comparison of TCR stimulation–associated CD107a levels without (–) or with SHP-1 inhibition (+). Paired 2-tailed *t* test; *** $P < 0.001$; **$P < 0.01$; *$P < 0.05$. Data were obtained from 6 independent experiments. (**B**) Relative CD107a degranulation ratio (in gMFI) obtained in the presence versus the absence of the SHP-1 inhibitor SSG. Graphs show relative CD107 fold increase following stimulation with unloaded (left panel) or NY-ESO-1–pulsed (right panel) T2 cells. (**C**) Melanoma cell killing by TCR-transduced CD8+ T cells without (mock) or with SSG treatment for 4 days. Tumor reactivity for the melanoma cell line Me 275 was assessed in a functional 4-hour ^{51}Cr release assay. (**D**) Relative ^{51}Cr cpm ratio with and without SSG at the indicated E:T ratios. Unpaired 2-tailed *t* test; ***$P < 0.001$; **$P < 0.01$; *$P < 0.05$.

ACT using autologous T lymphocytes reprogrammed by TCR gene transfer aims to confer robust immune reactivity toward defined tumor-associated antigen-bearing cells to which the endogenous T cell repertoire is weak or nonresponsive. Recently, 2 clinical trials were conducted whereby autologous T cells transduced with affinity-enhanced TCRs specific for tumor-associated antigens were adoptively transferred to patients with metastatic melanoma or sarcoma and demonstrated objective clinical responses (27, 28). Robbins and colleagues (28) were the first to examine the in vivo efficacy of adoptively transferred autologous T cells transduced with the sequence-optimized 1G4 TCR specific for NY-ESO-1$_{157-165}$. This genetically modified TCR possesses an affinity that lies just beyond the natural affinity range and confers maximal in vitro functionality with lowest cross-reactivity (6). In line with these observations, vaccination with peptide ligands of intermediate affinity yielded the most potent tumor-reactive CD8$^+$ T cells in vivo and best tumor growth control in BALB/c mice (15). Recently, Corse et al. further confirmed that peptide binding to the TCR with medium strength induced optimal in vivo CD4$^+$ T cell activation and subsequent immune responses (12). Future directions involve integrating the vast knowledge acquired from the in vitro experimental studies into the context of in vivo immune responses and clinical trials of ACT (reviewed in ref. 29).

The in silico structure-based approach allowed us to rationally design sequence substitutions in the CDR2α and/or CDR2β and/or CDR3β loops, known to interact either with the MHC surface or the bound peptide (Supplemental Table 1, refs. 8, 9; V. Zoete, M. Irving, and O. Michielin, unpublished observations). We also included in this panel the supraphysiological TCR variant wtc51m, previously identified by phage-display screening, with nanomolar range of affinity to the HLA-A2/NY-ESO-1 complex (30). Importantly, and despite their impaired functionality, all engineered CD8$^+$ T cells expressing supraphysiological TCRs of K_d < 1 μM (TMα, QMα, and wtc51m) retained a high degree of specificity toward the cognate pMHC target in functional assays (10, 11). An important finding in this study is that only engineered T cells with the highest TCR affinity variant (wtc51m) upregulated inhibitory receptors (PD-1 and BTLA) and conversely downregulated coactivatory receptors (CD28, HVEM, CD8β) (Figures 4 and 5). What remains intriguing is how such affine T cells control the expression of their activatory/inhibitory receptors readily under steady-state settings. One likely explanation is that, in contrast with the rational design approach (refs. 8, 9; V. Zoete, M. Irving, and O. Michielin, unpublished observations), gain in affinity for the wtc51m TCR variant resulted from multiple increased interactions with the HLA-A2 molecule, as this particular TCR contained up to 4 amino acid replacements within the CDR2β loop (30). Besides that, TCR surface expression also integrates and potentiates the effects of several variables/parameters including multiple coreceptors, TCR density, multivalent TCR clustering, and basal T cell activation state (reviewed in ref. 4). Together, weak but continuous TCR-A2–specific interactions regardless of the nature of the bound peptide may occur during the in vitro culture and periodic expansion of the transduced primary CD8$^+$ T cells and SUP-T1 cells (both HLA-A2 positive) and may be sufficient to modulate activatory/inhibitory receptor expression already under resting culture conditions. Notably, these conditions are very similar to the in vitro culture of autologous T cells transduced to express TCRs against HLA-A2/tumor antigens and further expanded before ACT (28). Collectively, these data emphasize the potential

impact of TCR-A2–binding affinity in relation to membrane receptor expression, T cell activation, and signaling, and highlight the need to carefully assess TCR affinity/avidity in relation to its functional efficacy for optimizing the design of ACT and vaccination.

An important aspect is to understand how T cells sense the differences in the strength of TCR peptide/MHC interactions, as observed here within the panel of affinity-optimized T cells. One of the current models (defined as the productive hit rate model) postulates that TCR-pMHC binding interactions need to be sufficiently long to initiate productive TCR signaling and subsequent T cell activation (reviewed in ref. 31). The model also indicates that TCR-pMHC bonds must be released quickly enough to enable serial triggering to acquire strong signals upon multiple interactions between TCRs and the pMHC complex. As a consequence, the productive hit rate model proposes that very fast or very slow TCR-pMHC dissociation rates would reduce the activation potential of T lymphocytes (14). The findings that maximal function occurred within a well-defined affinity window (K_d = 5 to 1 μM) and that above it, T cells engineered with supraphysiological TCR affinities responded less efficiently to antigen stimulation further support this model (11). Importantly, recent in vivo studies show that functional T cell responses are also largely influenced by TCR ligand affinity/avidity and the amount of presented antigen (12, 32). These observations are compatible with the notion that T cell clonotypes with a broad range of TCR affinities/avidities may participate equally (codominantly) in immune responses and that this may depend both on peptide-MHC potency and density (33).

Beside the biophysical regulation imposed by the TCR-pMHC binding parameters, the recruitment of inhibitory receptors like PD-1 in tumor-specific T cells of supraphysiological TCR affinity (wtc51m) reveals the presence of an additional level of control restraining effector function in those cells, such as observed in autoimmune or antitumoral responses. Engagement of PD-1 by PD-L1 is thought to be critical in preventing activation of self-reactive T cells that have escaped thymic clonal deletion (18). Accordingly, PD-1–deficient mice spontaneously develop autoimmune diseases (34), while in humans a regulatory polymorphism in PD-1 is associated with susceptibility to systemic lupus erythematosus and multiple sclerosis (35, 36). Induction of PD-L1 ligand expression has also been described in various tumor cells as a mechanism of cancer immune evasion (2). Furthermore, PD-1 expression is inducible in T cells following TCR stimulation and may be involved in the suppression of T cell activation in vitro and in vivo (37). However, the molecular basis by which PD-1 inhibits T cell activation is not fully understood. A recent study by Yokosuka and colleagues showed that upon PD-L1 binding, PD-1 could directly inhibit TCR-mediated signaling by recruiting SHP-2 phosphatase (38).

SHP-1 phosphatase negatively regulates TCR signal transduction and T cell activation upon TCR engagement and contributes to the setting of thresholds during thymocyte selection (19). Recently, SHP-1 was shown to limit the production of virus-specific effector CD8$^+$ T cells without having an impact on the formation of long-lived central memory cells (39). Furthermore, abrogation of SHP-1 expression in tumor-specific T cells improved efficacy of adoptive immunotherapy by enhancing the effector function and accumulation of short-lived effector T cells in vivo (40). Here, we extend these findings by showing that SHP-1 phosphatase may represent an important regulatory molecule in CD8$^+$ T cells with incremental affinity TCR variants. Importantly,

SHP-1 was found upregulated in a TCR affinity–dependent manner, with the highest levels in T cells with supraphysiological TCRs (Figure 6 and Supplemental Figure 5). This suggests that SHP-1 may play a dual role and restrict not only T cell signaling at the very low range of TCR stimulation (e.g., with antagonist ligands) as previously described (21), but also at the higher range (e.g., with optimized and supraphysiological TCR affinity ligands). Our observations are further consistent with a recent study showing that B cell receptor (BCR) signaling was limited by SHP-1 activity in the most proliferating germinal center B cells, revealing a regulatory effect on the affinity-based selection of those cells (41). However, additional studies using SHP-1–specific siRNA are still needed to fully demonstrate the impact of SHP-1 in mediating functional inhibition of affinity-optimized T cells.

Specific microRNAs have been shown to be critical for T cell development and function. For instance, transcriptional activation of miR-155 is detectable upon lymphocyte activation (42) and correlates with increased expression in human antigen-experienced CD8^{+} T cell subsets (23). Here, we provide evidence that miR-155 expression, but paradoxically not miR-181a expression, may be involved in modulating T cell function in TCR affinity–optimized CD8^{+} T cells. Thus, it will be of great importance to further explore the mechanisms by which miR-155 may influence cell activation and responsiveness along the TCR affinity range in peripheral T lymphocytes.

CTLA-4 and PD-1 are 2 checkpoint inhibitory receptors that have become novel targets for treating cancer patients, as these molecules can be specifically blocked with antibodies (43). Consequently, antibodies against PD-1 and PD-L1 have entered phase 1 clinical trials, and initial results showing objective tumor regression are highly promising (44, 45). More recently, 2 phase 1 trials using the phosphatase inhibitor SSG in combination with IFN-α2b have demonstrated safety and targeted inhibition in cancer patients (24, 25). Our findings highlight the critical role of SHP-1 expression among the whole panel of engineered CD8^{+} T cells. In particular, we show that targeting SHP-1 in T cells with optimal antitumor-specific TCRs (A97L, DMβ, and TMβ) further augments their functional efficacy. These observations provide the rationale for adoptive T cell therapy using affinity-optimized TCR variants combined with treatments blocking PD-1 and/or SHP1/2 phosphatases.

Methods

Cell lines and primary CD8^{+} T cells. TCR-α knockout SUP-T1 cells and HLA-A2^{+}/TAP-deficient T2 cells were cultured in RPMI supplemented with 10% FCS, 10 mM Hepes, penicillin (100 U/ml), and streptomycin (100 μg/ml). Human primary HLA-A2^{+} CD8^{+} T lymphocytes were obtained following positive enrichment using anti-CD8–coated magnetic microbeads (Miltenyi Biotec) and cultured in RPMI supplemented with 8% HS and 150 U/ml recombinant human IL-2. Cell-surface analysis and functional assays were performed between day 10 and 15 after stimulation with 30-Gy irradiated PBMCs as feeder cells and 1 μM PHA (Oxoid) as described previously (10).

NY-ESO-1–specific TCR αβ constructs, lentiviral production, and cell transduction. Cloning strategies and lentiviral production were performed as described previously (10, 11). The full-length codon-optimized TCR AV23.1 and TCR BV13.1 chain sequences of a dominant NY-ESO-1$_{157-165}$–specific T cell clone of patient LAU 155 were cloned in the pRRL, third generation lentiviral vectors, as an hPGK-AV23.1-IRES-BV13.1 construct. Structure-based amino acid substitutions were introduced into the WT TCR sequence using the QuikChange Mutagenesis Kit (Stratagene) and confirmed by DNA sequencing. Supernatant of lentiviral-transfected 293T cells was used to infect SUP-T1 or primary CD8^{+} T lymphocytes. PE-labeled A2/NY-ESO-1$_{157-165}$–specific multimers were used to sort transduced primary CD8^{+} T cells in order to enrich for multimer-positive cells by flow cytometry (FACS Vantage SE machine; BD Biosciences). Integrated lentiviral copy number was relatively equivalent for each one of the TCR variants within each type of transduced cell, i.e., 8 to 10 lentivirus copies/genome of SUP-T1 cells and 1 to 2 copies/genome of CD8^{+} T cells, as described in (11).

Flow cytometry analysis. Levels of NY-ESO-1–specific BV13.1/AV23 TCR expression on SUP-T1 and CD8^{+} T cells were monitored with PE-labeled NY-ESO-1$_{157-165}$–specific multimers (TC Metrix), FITC-conjugated BV13.1 antibody (Beckman Coulter), and FITC-conjugated pan–TCR-αβ antibodies (Beckman Coulter) before each experiment as previously described (10). For CD8 and TCR downregulation experiments, TCR-transduced CD8^{+} T cells were stimulated with 0.1 μg/ml unlabeled HLA-A2/NY-ESO-1$_{57-165}$–specific multimers for 4 hours at 37°C, before staining with FITC-labeled CD8 and PE-labeled A2/NY-ESO-1$_{157-165}$ multimers. The proportion (in percentages) of CD8^{+} T cells with reduced CD8 stainings as well as the MFI by multimer stainings were measured by flow cytometry (Gallios; Beckman Coulter). Staining of surface costimulatory molecules and coactivatory/inhibitory receptors was performed for 20 minutes at 4°C using the fluorophore-conjugated antibodies listed in Supplemental Methods. Intracellular stainings were performed according to the manufacturer's instructions. Data were acquired on a Gallios Flow Cytometer (Beckman Coulter) and analyzed using FlowJo (TreeStar).

Calcium flux assays upon NY-ESO-1 multimer stimulation. 5×10^4 TCR-transduced CD8^{+} T lymphocytes were loaded with 2 μM Indo 1-AM (Sigma-Aldrich) for 45 minutes at 37°C. Cells were washed and resuspended in 250 μl prewarmed RPMI containing 2% FCS. Baseline was recorded for 30 seconds before 1 μg/ml of unlabeled A2/NY-ESO-1 multimer was added to the cells. Intracellular Ca^{2+} flux was assessed over 5 minutes under UV excitation and constant temperature of 37°C using a thermostat device on a LSR II SORP (BD Biosciences) flow cytometer. Indo-1 (violet)/Indo-1 (blue) 405/525 nm emission ratio was analyzed by FlowJo kinetics module software (TreeStar).

Chromium release assays. Specific antigen recognition lytic activity of the NY-ESO-1–specific CD8^{+} T cells engineered with TCR variants of increased affinities was assessed functionally in 4-hour ^{51}Cr-release assays against the melanoma cell lines NA8 (HLA-A2[+]/NY-ESO-1^{−}) as well as Me 275 and Me 290 (HLA-A2[+]/NY-ESO-1^{+}). The percentage of specific lysis was calculated as follows: 100 × (experimental − spontaneous release)/(total − spontaneous release).

Microarray analysis. Primary CD8^{+} T cells (1×10^6) transduced with sequence-optimized NY-ESO-1–specific TCR variants were cultivated in RPMI supplemented with 8% HS and 10 U/ml rhIL-2 for 24 hours and left either unstimulated (baseline, 0 hour) or were stimulated with low dose 0.002 μg/ml unlabeled A2/NY-ESO-1$_{57-165}$–specific multimer for 6 hours at 37°C to avoid activation-induced cell death. The proportion of Annexin V^{+} cells was less than 10% (data not shown). After incubation, cells were washed with ice-cold PBS before quick freezing in liquid nitrogen. Frozen cell pellets were sent to Miltenyi Biotec GmbH and processed according to the vendor-recommended protocol for gene expression analysis as described in Supplemental Methods. The gene expression data described in this manuscript have been deposited in the NCBI Gene Expression Omnibus (GSE42922).

Western blot analysis. For all experiments, 1×10^6 untransduced or TCR-transduced SUP-T1 and primary CD8^{+} T cells were either left unstimulated (baseline) or stimulated with 10 g/ml unlabeled A2/NY-ESO-1$_{157-165}$ multimers for the indicated time in a 37°C water bath before washing with ice-cold PBS and quick freezing in liquid nitrogen. Following cell extraction, proteins were separated by SDS-PAGE and subsequently probed with the following primary antibodies: goat anti–SHP-1 (C-19) (LabForce AG), rabbit anti-pERK1/2 (Thr202/Tyr204) (D13.14.4E), mouse anti-ERK1/2 (3A7), rabbit anti–pZAP-70

(Tyr319)/Syk(Tyr352), rabbit anti–ZAP-70 (99F2) (Cell Signaling Technology), rabbit anti–pSHP-1 (Tyr536) (ECM Biosciences), mouse anti–α-tubulin (B-5-1-2) (Sigma-Aldrich), and rabbit anti-actin (AA20-33) (Sigma-Aldrich). Quantification of specific bands was done using PhosphoImager software (ImageJ) and normalized to α-tubulin or actin expression levels.

Quantitative PCR analysis for miR-155 and miR-181a expression. TCR-transduced CD8^{+} T cells (1×10^6) were left either unstimulated (baseline, 0 hour) or stimulated with 0.01 µg/ml unlabeled A2/NY-ESO-1$_{157-165}$ multimers for 6, 24, and 48 hours at 37°C under 10 U/ml rhIL-2 medium conditions. Following incubation, cells were washed and total RNA was extracted with the miRVana kit (Ambion; Life Technologies), and mature microRNAs (hsa-miR-155, hsa-miR-181a, and hsa-RNU48) were reverse transcribed with the TaqMan MicroRNA Reverse Transcription Kit (Applied Biosystems). Amplification and real-time acquisition were performed using Universal PCR Master Mix (Applied Biosystems) in MicroAmp 384-well plates (Applied Biosystems) on a LightCycler 480 instrument (Roche Ltd.). Ct (RNU48) was subtracted from Ct (miR-155, miR-181a) to calculate relative expression (ΔCt).

Functional PD-L1 blockade or pharmacological SHP-1/SHP-2 inhibition assays. For PD-L1 blockade, 5×10^5 TCR-transduced CD8^{+} T cells were cultured in 500 µl RPMI complemented with 8% HS, 150 U/ml rhIL-2 at 37°C without (control) or with 5 µg/ml PD-L1 blocking antibody (CD274 clone MIH1; eBioscience). Alternatively, 50 µg/ml SSG (Sb content; Santa Cruz Biotechnology Inc.) was used for SHP-1/SHP-2 inhibition. After 3–4 days, 4×10^5 T cells were incubated at 37°C for 4 hours with 2×10^5 either unloaded T2 (control) or 10 µM NY-ESO-1–loaded T2 cells (E:T ratio 2:1) together with PE-Cy5 CD107a/LAMP-1 (BD Biosciences) antibody. Acquisition was performed on an LSRI (BD Biosciences) or a Gallios (Beckman Coulter) instrument, and data were analyzed with FlowJo (TreeStar). For target cell killing experiments, TCR-transduced CD8^{+} T cells were incubated with 50 µg/ml SSG for 3–4 days as described above before assessing antigen-specific lytic activity in a 4-hour ^{51}Cr-release assay against Me 275 cells (HLA-A2[+]/NY-ESO-1^{+}) at 10:1 and 3:1 effector/target (E:T) ratios.

Statistics. For quantitative comparison, paired or unpaired Student's *t* test (2-sample, 2-tailed comparison), as indicated, was performed using GraphPad Prism software; $P < 0.05$ was considered significant.

Study approval. Human peripheral blood cells were obtained from healthy donors of the Blood Transfusion Center of the University of Lausanne. All donors had previously completed the Swiss National Medical questionnaire to verify that they fulfilled the criteria for blood donation and provided written informed consent for the use of blood samples in medical research after anonymization.

Address correspondence to: Nathalie Rufer, Ludwig Center for Cancer Research, University of Lausanne, c/o HO, niv 5, Avenue Pierre-Decker 4, CH-1011 Lausanne, Switzerland. Phone: 41.21.314.01.99; Fax: 41.21.314.74.77; E-mail: Nathalie.Rufer@unil.ch.

Lukas Baitsch's present address is: Department of Cancer Biology, Dana Farber Cancer Institute, and Department of Biological Chemistry and Molecular Pharmacology, Harvard Medical School, Boston, Massachusetts, USA.

1. Davis MM, et al. Dynamics of cell surface molecules during T cell recognition. *Annu Rev Biochem*. 2003; 72:717–742.
2. Schreiber RD, Old LJ, Smyth MJ. Cancer immunoediting: integrating immunity's roles in cancer suppression and promotion. *Science*. 2011; 331(6024):1565–1570.
3. Uttenthal BJ, Chua I, Morris EC, Stauss HJ. Challenges in T cell receptor gene therapy. *J Gene Med*. 2012;14(6):386–399.
4. Stone JD, Chervin AS, Kranz DM. T-cell receptor binding affinities and kinetics: impact on T-cell activity and specificity. *Immunology*. 2009; 126(2):165–176.
5. Zhao Y, et al. High-affinity TCRs generated by phage display provide CD4+ T cells with the ability to recognize and kill tumor cell lines. *J Immunol*. 2007; 179(9):5845–5854.
6. Robbins PF, et al. Single and dual amino acid substitutions in TCR CDRs can enhance antigen-specific T cell functions. *J Immunol*. 2008;180(9):6116–6131.
7. Holler PD, Chlewicki LK, Kranz DM. TCRs with high affinity for foreign pMHC show self-reactivity. *Nat Immunol*. 2003;4(1):55–62.
8. Zoete V, Michielin O. Comparison between computational alanine scanning and per-residue binding free energy decomposition for protein-protein association using MM-GBSA: application to the TCR-p-MHC complex. *Proteins*. 2007;67(4):1026–1047.
9. Zoete V, Irving MB, Michielin O. MM-GBSA binding free energy decomposition and T cell receptor engineering. *J Mol Recognit*. 2010;23(2):142–152.
10. Schmid DA, et al. Evidence for a TCR affinity threshold delimiting maximal CD8 T cell function.

J Immunol. 2010;184(9):4936–4946.
11. Irving M, et al. Interplay between T cell receptor binding kinetics and the level of cognate peptide presented by major histocompatibility complexes governs CD8+ T cell responsiveness. *J Biol Chem*. 2012;287(27):23068–23078.
12. Corse E, Gottschalk RA, Krogsgaard M, Allison JP. Attenuated T cell responses to a high-potency ligand in vivo. *PLoS Biol*. 2010;8(9):pii:e1000481.
13. Gonzalez PA, et al. T cell receptor binding kinetics required for T cell activation depend on the density of cognate ligand on the antigen-presenting cell. *Proc Natl Acad Sci U S A*. 2005;102(13):4824–4829.
14. Kalergis AM, et al. Efficient T cell activation requires an optimal dwell-time of interaction between the TCR and the pMHC complex. *Nat Immunol*. 2001;2(3):229–234.
15. McMahan RH, McWilliams JA, Jordan KR, Dow SW, Wilson DB, Slansky JE. Relating TCR-peptide-MHC affinity to immunogenicity for the design of tumor vaccines. *J Clin Invest*. 2006;116(9):2543–2551.
16. Thomas S, Xue SA, Bangham CR, Jakobsen BK, Morris EC, Stauss HJ. Human T cells expressing affinity-matured TCR display accelerated responses but fail to recognize low density of MHC-peptide antigen. *Blood*. 2011;118(2):319–329.
17. Watanabe N, et al. BTLA is a lymphocyte inhibitory receptor with similarities to CTLA-4 and PD-1. *Nat Immunol*. 2003;4(7):670–679.
18. Fife BT, Pauken KE. The role of the PD-1 pathway in autoimmunity and peripheral tolerance. *Ann N Y Acad Sci*. 2011;1217:45–59.
19. Lorenz U. SHP-1 and SHP-2 in T cells: two phosphatases functioning at many levels. *Immunol Rev*.

2009;228(1):342–359.
20. Zhang Z, Shen K, Lu W, Cole PA. The role of C-terminal tyrosine phosphorylation in the regulation of SHP-1 explored via expressed protein ligation. *J Biol Chem*. 2003;278(7):4668–4674.
21. Stefanova I, Hemmer B, Vergelli M, Martin R, Biddison WE, Germain RN. TCR ligand discrimination is enforced by competing ERK positive and SHP-1 negative feedback pathways. *Nat Immunol*. 2003;4(3):248–254.
22. Li QJ, et al. miR-181a is an intrinsic modulator of T cell sensitivity and selection. *Cell*. 2007; 129(1):147–161.
23. Salaun B, et al. Differentiation associated regulation of microRNA expression in vivo in human CD8+ T cell subsets. *J Transl Med*. 2011;9:44.
24. Yi T, et al. Phosphatase inhibitor, sodium stibogluconate, in combination with interferon (IFN) alpha 2b: phase I trials to identify pharmacodynamic and clinical effects. *Oncotarget*. 2011;2(12):1155–1164.
25. Naing A, et al. Phase I dose escalation study of sodium stibogluconate (SSG), a protein tyrosine phosphatase inhibitor, combined with interferon alpha for patients with solid tumors. *J Cancer*. 2011; 2:81–89.
26. Pathak MK, Yi T. Sodium stibogluconate is a potent inhibitor of protein tyrosine phosphatases and augments cytokine responses in hemopoietic cell lines. *J Immunol*. 2001;167(6):3391–3397.
27. Johnson LA, et al. Gene therapy with human and mouse T-cell receptors mediates cancer regression and targets normal tissues expressing cognate antigen. *Blood*. 2009;114(3):535–546.
28. Robbins PF, et al. Tumor regression in patients with

29. Corse E, Gottschalk RA, Allison JP. Strength of TCR-peptide/MHC interactions and in vivo T cell responses. *J Immunol*. 2011;186(9):5039–5045.

30. Dunn SM, et al. Directed evolution of human T cell receptor CDR2 residues by phage display dramatically enhances affinity for cognate peptide-MHC without increasing apparent cross-reactivity. *Protein Sci*. 2006;15(4):710–721.

31. Valitutti S. The serial engagement model 17 years after: From TCR triggering to immunotherapy. *Front Immunol*. 2012;3:272.

32. Zehn D, Lee SY, Bevan MJ. Complete but curtailed T-cell response to very low-affinity antigen. *Nature*. 2009;458(7235):211–214.

33. Gottschalk RA, et al. Distinct influences of peptide-MHC quality and quantity on in vivo T-cell responses. *Proc Natl Acad Sci U S A*. 2012;109(3):881–886.

34. Nishimura H, et al. Autoimmune dilated cardiomyopathy in PD-1 receptor-deficient mice. *Science*. 2001;291(5502):319–322.

35. Kroner A, et al. A PD-1 polymorphism is associated with disease progression in multiple sclerosis. *Ann Neurol*. 2005;58(1):50–57.

36. Prokunina L, et al. A regulatory polymorphism in PDCD1 is associated with susceptibility to systemic lupus erythematosus in humans. *Nat Genet*. 2002;32(4):666–669.

37. Keir ME, Butte MJ, Freeman GJ, Sharpe AH. PD-1 and its ligands in tolerance and immunity. *Annu Rev Immunol*. 2008;26:677–704.

38. Yokosuka T, Takamatsu M, Kobayashi-Imanishi W, Hashimoto-Tane A, Azuma M, Saito T. Programmed cell death 1 forms negative costimulatory microclusters that directly inhibit T cell receptor signaling by recruiting phosphatase SHP2. *J Exp Med*. 2012;209(6):1201–1217.

39. Fowler CC, Pao LI, Blattman JN, Greenberg PD. SHP-1 in T cells limits the production of CD8 effector cells without impacting the formation of long-lived central memory cells. *J Immunol*. 2010; 185(6):3256–3267.

40. Stromnes IM, et al. Abrogation of SRC homology region 2 domain-containing phosphatase 1 in tumor-specific T cells improves efficacy of adoptive immunotherapy by enhancing the effector function and accumulation of short-lived effector T cells in vivo. *J Immunol*. 2012;189(4):1812–1825.

41. Khalil AM, Cambier JC, Shlomchik MJ. B cell receptor signal transduction in the GC is short-circuited by high phosphatase activity. *Science*. 2012; 336(6085):1178–1181.

42. Haasch D, et al. T cell activation induces a noncoding RNA transcript sensitive to inhibition by immunosuppressant drugs and encoded by the proto-oncogene, BIC. *Cell Immunol*. 2002; 217(1–2):78–86.

43. Pardoll D, Drake C. Immunotherapy earns its spot in the ranks of cancer therapy. *J Exp Med*. 2012;209(2):201–209.

44. Brahmer JR, et al. Safety and activity of anti-PD-L1 antibody in patients with advanced cancer. *N Engl J Med*. 2012;366(26):2455–2465.

45. Topalian SL, Drake CG, Pardoll DM. Targeting the PD-1/B7-H1(PD-L1) pathway to activate anti-tumor immunity. *Curr Opin Immunol*. 2012; 24(2):207–212.

(metastatic synovial cell sarcoma and melanoma using genetically engineered lymphocytes reactive with NY-ESO-1. *J Clin Oncol*. 2011;29(7):917–924.)